### GAITGen: Disentangled Motion-Pathology Impaired Gait Generative Model – Bringing Motion Generation to the Clinical Domain

Vida Adeli<sup>1,2,3</sup>, Soroush Mehraban<sup>2,3,4</sup>, Majid Mirmehdi<sup>5</sup>, Alan Whone<sup>6</sup>, Benjamin Filtjens<sup>2,3,7</sup>, Amirhossein Dadashzadeh<sup>5</sup>, Alfonso Fasano<sup>3,8,9,10</sup>, Andrea Iaboni<sup>3,11,12</sup>, Babak Taati<sup>1,2,3,4</sup>

<sup>1</sup>University of Toronto, Computer Science Department <sup>2</sup>Vector Institute

<sup>3</sup> KITE Research Institute, UHN <sup>4</sup>University of Toronto, Institute of Biomedical Engineering

<sup>5</sup>University of Bristol, School of Computer Science <sup>6</sup>University of Bristol, Translational Health Science

<sup>7</sup>University of Toronto, Data Sciences Institute <sup>8</sup>University of Toronto, Department of Medicine, Division of Neurology

<sup>9</sup> Krembil Research Institute, UHN <sup>10</sup>Edmond J. Safra Program in Parkinson's Disease, UHN

<sup>11</sup>University of Toronto, Department of Psychiatry <sup>12</sup>Centre for Mental Health, UHN https://vadeli.github.io/GAITGen/

## Abstract

Gait analysis is crucial for the diagnosis and monitoring of movement disorders like Parkinson's Disease. While computer vision models have shown potential for objectively evaluating parkinsonian gait, their effectiveness is limited by scarce clinical datasets and the challenge of collecting large and well-labelled data, impacting model accuracy and risk of bias. To address these gaps, we propose GAITGen, a novel framework that generates realistic gait sequences conditioned on specified pathology severity levels. GAITGen employs a Conditional Residual Vector Quantized Variational Autoencoder to learn disentangled representations of motion dynamics and pathology-specific factors, coupled with Mask and Residual Transformers for conditioned sequence generation. GAITGen generates realistic, diverse gait sequences across severity levels, enriching datasets and enabling large-scale model training in parkinsonian gait analysis. Experiments on our new PD-GaM (real) dataset demonstrate that GAITGen outperforms adapted state-of-the-art models in both reconstruction fidelity and generation quality, accurately capturing critical pathology-specific gait features. A clinical user study confirms the realism and clinical relevance of our generated sequences. Moreover, incorporating GAITGengenerated data into downstream tasks improves parkinsonian gait severity estimation, highlighting its potential for advancing clinical gait analysis.

#### 1. Introduction

Gait analysis is essential in the assessment of movement disorders such as Parkinson's Disease (PD). Computer vi-

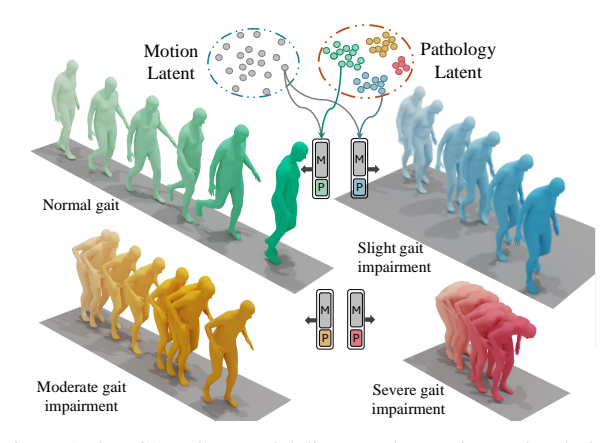


Figure 1. Our GAITGen model disentangles motion and pathology into distinct latents, allowing the same motion dynamics to present differently across pathology latents. This disentanglement enables controlled generation of gait sequences conditioned on pathology levels.

sion models have been developed to objectively evaluate parkinsonian gait using videos of older adults walking, representing significant progress toward more accurate and accessible assessments [12, 25, 31, 32, 46]. Despite these advances, current models face several challenges that limit their effectiveness [2]. Developing robust machine learning models requires extensive training data. However, collecting large and diverse gait video datasets is resource-intensive and raises privacy concerns for patients, often resulting in limited and demographically skewed datasets [8, 25, 34, 43]. People with severe parkinsonian gait are particularly underrepresented in these datasets. This scarcity impacts model performance and raises concerns about bias and generalizability across different populations [61]. Moreover, variability in ratings among clinicians introduces in-

consistencies in gait severity scoring, affecting the reliability of ground truth labels used for training and evaluation [10, 44]. The severity of gait impairments in PD is commonly assessed using the Unified Parkinson's Disease Rating Scale (UPDRS) [16]. We focus on the UPDRS Part III gait subscore, hereafter referred to as UPDRS-gait. This scale rates symptoms on a scale from 0 (normal) to 4 (severe impairment). Some of the gait symptoms of PD include small steps and shuffling gait, slow speed, reduced arm swing, stooped posture, and narrow base of support [23, 36].

Generating clinically relevant gait data conditioned on specific pathology severity levels could address existing challenges by augmenting limited real datasets, especially for underrepresented severe cases. However, this task poses significant difficulties due to the complexity of capturing pathology-specific characteristics and ensuring the generated data is clinically relevant. Existing motion generative models [6, 18, 41] fail to capture nuanced gait deviations associated with movement disorders. Moreover, while large datasets exist for general motion tasks [17, 42], none are suited for generating motions that capture pathologyspecific characteristics of impaired gait. Existing gait abnormality datasets are typically small [43] and not formatted for these generative models. Additionally, there is no prior work on generating clinically relevant motions, and standard text-to-motion evaluation metrics previously used [6, 51] are inadequate for this specialized task. To address these gaps, new clinically relevant metrics need to be introduced that assess targeted pathological characteristics, with the flexibility to be adapted for other clinically significant factors. This paper establishes a foundation for assessing generative models in clinical motion analysis.

Our proposed model, GAITGen, is the first to approach the clinically relevant task of generating realistic, pathology-conditioned gait sequences. GAITGen employs a Conditional Residual Vector Quantized Variational Autoencoder (RVQ-VAE) with specific mechanisms to enforce disentanglement, along with a Mask Transformer and a Residual Transformer for conditioned sequence generation. This disentanglement further allows us to leverage motions with mild or moderate impairment and impose severe impairment characteristics, effectively augmenting the dataset with diverse samples across all severity levels (Fig. 1).

Our main contributions are: 1) We propose **GAITGen**, a novel model for generating synthetic, clinically relevant gait sequences conditioned on pathology levels by learning disentangled representation of motion and pathology. This representation also enables Mix and Match augmentation, where pathology characteristics can be superimposed onto different motion profiles. 2) We introduce **PD-GaM**, a public 3D mesh dataset of gait sequences with UPDRS-gait scores along with new evaluation metrics tailored for the pathology-conditioned gait generation task, establishing a

foundation for assessing generative models in clinical motion analysis. 3) We validate our model's clinical relevance and downstream impact through clinician evaluations that confirm the realism and clinical relevance of our synthetic sequences. Using GAITGen-generated data for downstream task improves parkinsonian severity estimation, highlighting its potential utility in clinical applications.

#### 2. Related Works

Human Motion Synthesis. Recently, text-conditioned human motion synthesis has been widely studied [6, 9, 18, 51, 63, 64]. MDM [51] proposes a conditional diffusion model for motion synthesis. MLD [6] reduces the computational overhead and enhances the quality of MDM by leveraging a Variational Autoencoder and a compact representation for motion sequences. MotionLCM [9] uses a consistency model to improve runtime efficiency of MLD and adds a motion ControlNet to add additional control such as setting an initial pose. MoMask [18] introduces a residual VQ-VAE to represent motion sequences in a lowdimensional space and then uses a mask modeling approach with transformers to synthesize motions. OmniControl [60] adds more control to the motion generation by including a flexible spatial control signal over different body joints at different times. Although these methods perform remarkably well in generating human motion aligned with text conditions, they struggle to generate clinically specific unseen motion sequences, such as pathological gait patterns. Furthermore, their success depends on exposure to a large number of samples during training, which is not feasible for datasets involving walking patients with PD.

Human Motion Style Transfer. These methods transfer style from one motion sequence to another while preserving the motion content of the original motion sequence [1, 4, 49, 50, 62]. Aberman et al. [1] use separate encoders for motion content and style, reconstructing motion from content while modifying style via adaptive instance normalization (AdaIN). Cheng et al. [4] propose an end-to-end training using a diffusion model to generate a motion by controlling the style. Style-ERD [50] introduces a new online style transfer model to work in real time. MCM-LDM [49] proposes a novel model for arbitrary motion style transfer, effectively integrating content, style, and trajectory to produce cohesive motion animations. CycleDance [62] introduces a cross-modal transformer-based framework for unpaired dance style transfer that incorporates music context to enhance motion style realism. Unlike style, pathology in gait is not merely a superficial attribute but fundamentally affects the underlying motion dynamics and biomechanical patterns of walking. Beyond the style of walking, it influences factors such as speed, walking distance, or freezing of gait mid-stride. Modeling pathology as a style fails to capture the complex interactions between pathology and mo-

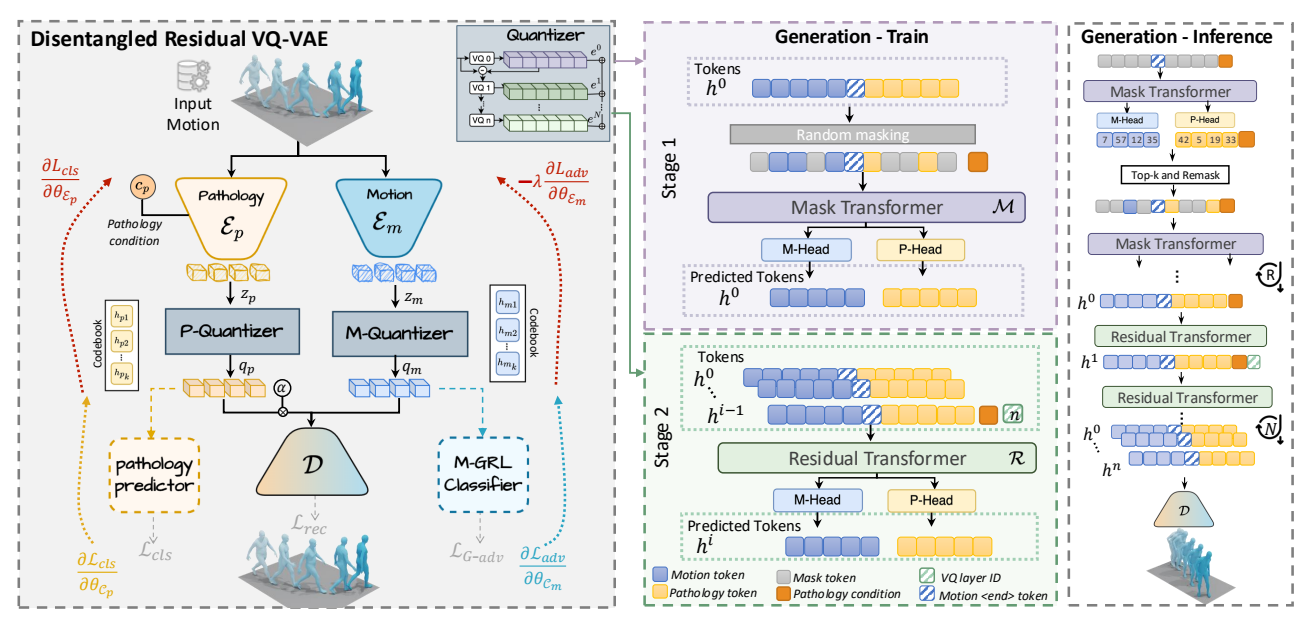


Figure 2. GAITGen architecture. 1) Disentangled Residual VQ-VAE encodes gait sequences into separate motion ( $\mathcal{E}_m$ ) and pathology ( $\mathcal{E}_p$ ) latents, enforced by distinct quantizers and classifiers for disentanglement. 2) Generation - Train: In the first stage of training, masked motion and pathology tokens are generated using the Mask Transformer ( $\mathcal{M}$ ) with separate heads for each latent. In the second stage, the Residual Transformer ( $\mathcal{R}$ ) predicts residuals with a next layer prediction task. 3) During inference,  $\mathcal{M}$  predicts masked tokens iteratively, followed by the  $\mathcal{R}$ , which incrementally refines the representations across multiple quantization layers, conditioned on the pathology level.

tion, resulting in unrealistic or implausible gait sequences that do not accurately represent pathological gait.

Disentanglement in Generation. Disentangling two concepts is crucial for achieving precise control over highquality generation [3, 21, 26, 54–56, 59]. Previous research has shown disentanglement, when used on downstream tasks, enhances predictive performance [28, 29], offers interpretability [19], reduces sample complexity [45, 53], and improves fairness [27]. In generative domain, G<sup>3</sup>AN [55] disentangles human motion and appearance for realistic human video generation. DiffSFSR [26] learns disentangled representations for background, face identity, and facial expression for personalized face generation. Similarly, DisCo [54] disentangles subject and background for realistic human dance generation. Although disentanglement of two factors has not been studied in human motion generation, we believe that separating pathology from motion content is crucial for generating high-quality gait sequences that accurately reflect the specified pathology condition. Synthetic Data as Augmentation. A large body of research has demonstrated the utility of synthetic data in augmenting limited real training data [22, 38, 47, 47, 56, 57], even where synthetic data does not look realistic [20, 37]. By disentangling pathology and motion in gait sequences, we show that the resulting synthetic data can significantly enhance model accuracy, that may impact clinical research into earlier diagnosis of PD. Previously, [5] attempted to address data scarcity in PD severity estimation by basic interpolation of 2D skeletal data. However, it falls short of capturing the complex, pathology-specific characteristics of parkinsonian gait.

#### 3. Method

Given a gait sequence  $\mathbf{x} \in \mathbb{R}^{T \times D}$  with a corresponding pathology severity label  $c_p \in \{0, \dots, C-1\}$ , where T denotes the sequence length, D the dimensionality of the motion representation, and C the number of pathology severity classes (hereafter referred to as "pathology" for brevity), our goal is, 1) to learn a disentangled representation that separates motion dynamics from pathologyspecific factors, ensuring high reconstruction fidelity and information preservation; 2) to build a generative model capable of synthesizing gait sequences conditioned on pathology levels, enabling a detailed analysis of pathology impact on gait dynamics. To achieve these goals, we propose GAIT-Gen, a model that combines a Conditional Residual Vector Quantized Variational Autoencoder with specific mechanisms to enforce disentanglement (Sec. 3.1.1), along with a Mask Transformer (Sec. 3.1.2) and Residual Transformer (Sec. 3.1.3) for conditional gait generation.

#### 3.1. GAITGen Architecture

The overall architecture is illustrated in Fig. 2. We emphasize why a disentanglement is essential in the first place. Given the limited number of samples in severe pathology classes (often only a few participants), training a generative model to produce diverse motions for these cases is not trivial. Disentangling motion from pathology allows us to

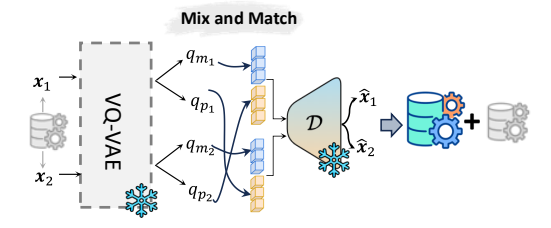


Figure 3. Mix and Match augmentation. Motion latent codes  $(q_m)$  from one sample are combined with pathology latent codes  $(q_p)$  from another to synthesize new gait sequences.

learn diverse motion patterns from the more abundant, less severe cases, and then impose the characteristics of severe pathology onto these motions to obtain a more varied data distribution samples for severe conditions.

#### 3.1.1. Motion-Pathology Disentangled RVQ-VAE

To learn disentangled representations of motion and pathology, we employ a Conditional Residual VQ-VAE with two encoders: one for motion and one for pathology.

**Encoders.** The motion encoder  $\mathcal{E}_m$  encodes the input motion sequence  $\mathbf{x} \in \mathbb{R}^{T \times D}$  into a latent representation  $\mathbf{z}_m = \mathcal{E}_m(\mathbf{x}) \in \mathbb{R}^{T' \times D_m}$ , aiming to capture pathology-invariant motion dynamics. The pathology encoder,  $\mathcal{E}_p$ , is a *conditional* encoder that generates a latent representation  $\mathbf{z}_p = \mathcal{E}_p(\mathbf{x}, c_p) \in \mathbb{R}^{T' \times D_p}$ , conditioned on the pathology severity level  $c_p$ . This conditioning pushes class representations apart in the pathology latent space, enhancing the separability between severity levels and improving the model's ability to capture varying degrees of pathology more effectively. Here, T' represents the downsampled temporal dimensions, while  $D_m$  and  $D_p$  are the embedding dimensions of the respective latents.

Residual Vector Quantization. We employ Residual Vector Quantization (RVQ) in the motion and pathology encoders to capture hierarchical and discrete features at multiple levels of abstraction. By quantizing the latent space, we constrain the representations to a discrete set of physically plausible pose configurations, which stabilizes training by reducing gradient variance and leading to faster convergence. RVO operates by sequentially quantizing the residuals between the input and the output from previous quantization layers. This process allows the model to capture both coarse and fine-grained gait patterns, enhancing the representational capacity of the latent features. Let  $k \in \{m, p\}$ denote the corresponding motion or pathology latent space and  $n \in N$  represent quantization layer index. The initial latent  $\mathbf{z}_k$  is quantized to obtain the first quantized embedding  $\mathbf{e}_k^{(0)}$  and codebook indices  $\mathbf{h}_k^{(0)}$ . Then the residual  $\mathbf{r}_k^{(0)}$  is computed by the error between  $\mathbf{e}_k^{(0)}$  and  $\mathbf{z}_k$ :

$$\mathbf{e}_k^{(0)} = \text{Quantize}(\mathbf{z}_k), \qquad \mathbf{r}_k^{(0)} = \mathbf{z}_k - \mathbf{e}_k^{(0)}$$
 (1)

For each subsequent quantization layer n, the residual from the previous layer  $\mathbf{r}_k^{(n-1)}$  is quantized to obtain the quantized

tized embedding  $\mathbf{e}_k^{(n)}$ , and a new residual  $\mathbf{r}_k^{(n)}$ :

$$\mathbf{e}_{k}^{(n)} = \text{Quantize}(\mathbf{r}_{k}^{(n-1)}) \quad \mathbf{r}_{k}^{(n)} = \mathbf{r}_{k}^{(n-1)} - \mathbf{e}_{k}^{(n)}$$
 (2)

The final latent representation  $\mathbf{q}_k$  for latent k is obtained by summing all the quantized embeddings from the layers:  $\mathbf{q}_k = \sum_{n=1}^N \mathbf{e}_k^{(n)}$ . This hierarchical quantization ensures that both global and local features are effectively captured.

**Decoder.** Finally, the decoder  $\mathcal{D}$  reconstructs the input gait sequence from the combined motion and pathology latent representations,  $\hat{\mathbf{x}} = \mathcal{D}(\mathbf{q}_m + \alpha \cdot \mathbf{q}_p)$ , where  $\alpha$  is an interference weight that modulates the level of pathology integrated into the reconstruction.

Training and disentanglement enforcement. To achieve disentanglement, we design the training procedure so that the motion encoder captures only pathology-invariant features, while the pathology encoder isolates pathologyspecific details. We begin by first pretraining only the motion encoder  $\mathcal{E}_m$  with the decoder  $\mathcal{D}$  using reconstruction losses. This ensures that  $\mathbf{q}_m$  captures essential motion features needed for accurate gait reconstruction and contains plausible motion representations even without contributions from the pathology latent. Following this pretraining phase, we introduce the pathology encoder  $\mathcal{E}_p$  and continue finetuning  $\mathcal{E}_m$  with a reduced learning rate, ensuring that it retains the motion features while gradually unlearning any pathology-related information. To restrict  $\mathcal{E}_p$  from encoding non-essential pathology details, it is designed with fewer codebooks than  $\mathcal{E}_m$ , limiting its capacity to encode irrelevant features. For healthy gait sequences ( $c_p = 0$ ), pathology features  $\mathbf{q}_p$  are zeroed out during training, forcing  $\mathcal{E}_m$ to capture all necessary motion information for reconstruction. With no contribution from  $q_p$ , any reconstruction errors must be corrected by the motion latent alone.

The reconstruction loss is calculated combining two terms ( $\mathcal{L}_{rec} = \mathcal{L}_{pos} + \mathcal{L}_{geo}$ ), where  $\mathcal{L}_{pos}$  is the MAE for the input features excluding rotational components:

$$\mathcal{L}_{pos} = ||\mathbf{x}_{\neg rot} - \mathbf{\hat{x}}_{\neg rot}||_{1} \quad (\mathbf{x}_{\neg rot} = \mathbf{x} \setminus \mathbf{x}_{rot})$$
(3)

For rotational components, a geodesic distance loss is applied ensuring rotation comparisons respect the non-Euclidean SO(3) manifold. First, 6D joint rotations are converted to rotation matrices  $\mathbf{x}_R$  using the Gram-Schmidt process [65]. Then the geodesic loss is computed as:

$$\mathcal{L}_{\text{geo}} = \sum^{T} \arccos \left( \frac{\text{Tr}(\mathbf{x}_{R} \left( \hat{\mathbf{x}}_{R}^{-1} \right)) - 1}{2} \right)$$
(4)

To further enforce the disentanglement and prevent information leakage, two auxiliary classifiers are applied on the quantized latents. First, latents are processed through a self-attention block to aggregate channel information: ( $\mathbf{f}_k = \mathrm{SelfAttn}(\mathbf{q}_k)$ ). Then, the pathology classifier  $\phi_p$  predicts severity from the pathology latent, while an adversarial pathology classifier  $\psi_m$  on the motion latent, using a

gradient reversal layer (GRL) [14], encourages motion latent invariance to pathology. The classification ( $\mathcal{L}_{cls}$ ) and adversarial ( $\mathcal{L}_{G-adv}$ ) losses are defined as follows:

$$\mathcal{L}_{cls} = \mathbb{E}_{(\mathbf{f}_p, c_p) \sim \mathcal{D}}[\ell_{CE}(\phi_p(\mathbf{f}_p), c_p)]$$
 (5)

$$\mathcal{L}_{\text{G-adv}} = \mathbb{E}_{(\mathbf{f}_m, c_p) \sim \mathcal{D}}[\ell_{\text{CE}}(\psi_m(\text{GRL}(\mathbf{f}_m)), c_p)]$$
 (6)

The total training objective integrates all loss terms:

$$\mathcal{L}_{vq} = \lambda_r \mathcal{L}_{rec} + \lambda_c \mathcal{L}_{cls} + \lambda_{adv} \mathcal{L}_{adv} + \lambda_{emb} \mathcal{L}_{emb}, \tag{7}$$

with an embedding loss at each quantization layer for both latents.

$$\mathcal{L}_{\text{emb}} = \sum_{k \in \{m, p\}} \sum_{n=1}^{N} ||\mathbf{r}_{k}^{(n)} - \text{sg}[\mathbf{e}_{k}^{(n)}]||_{2}^{2}.$$
 (8)

where  $sg[\cdot]$  denotes the stop-gradient operation. Codebooks are updated using exponential moving averages and codebook reset strategies [63].

#### 3.1.2. Masked Transformer

To generate gait sequences conditioned on pathology, we use a bidirectional Mask Transformer  $(\mathcal{M}_{\theta})$  on the first-layer quantized latents from the disentangled RVQ-VAE. This approach has proven effective in learning VQ-VAE codebook structure and enables efficient inference while producing high-quality samples, as demonstrated in [18]. Our Mask Transformer is designed to simultaneously process both motion and pathology latent tokens within a single model. A special end-of-motion token, <MEND>, is defined to delineate motion and pathology tokens. This structure enables  $\mathcal{M}_{\theta}$  to differentiate and selectively attend to motion and pathology tokens [13, 66].

We train  $\mathcal{M}_{\theta}$  using a masked token modeling approach inspired by BERT [24]. Given the concatenated tokens  $\mathbf{h}^{(0)} = [\mathbf{h}_m^{(0)}; <\text{MEND>}; \mathbf{h}_p^{(0)}] \in \mathbb{R}^{(2T'+1)\times d}$  from the first quantization layer, where  $\mathbf{h}_m$  and  $\mathbf{h}_p$  are projected to a common dimension d, we randomly mask a subset of tokens based on a cosine noise schedule  $\beta(t)$ . The model predicts the original tokens at the masked positions, minimizing the cross-entropy loss ( $\mathcal{L}_{\text{mTrans}}$ ), where  $\tilde{m}$  represents the set of masked token indices and  $\tilde{\mathbf{h}}$  is the masked sequence.

$$\mathcal{L}_{\text{mTrans}} = -\sum_{i \in \tilde{m}} \log \mathcal{M}_{\theta}(\mathbf{h}_{i}^{(0)} \mid \tilde{\mathbf{h}}, c_{p})$$
 (9)

During inference, starting from a fully masked sequence,  $\mathcal{M}_{\theta}$  iteratively generates the base-layer tokens by predicting masked tokens conditioned on pathology  $c_p$ . At each step, it selects high-confidence tokens, re-masks low-confidence ones, and continues this refinement over R steps.

#### 3.1.3. Residual Transformer

A single bidirectional residual transformer  $(\mathcal{R}_{\theta})$  is used to generate residuals in the RVQ-VAE by predicting the next layer residuals given previous layers. At each quantization layer n,  $\mathcal{R}_{\theta}$  takes cumulative embedded tokens  $\mathbf{h}_{k}^{(0:n-1)}$ 

Method	AVE ↓	<b>AAMD</b> ↓	ASMD ↓	$\mathbf{Div} \rightarrow$
Real	-	-	-	3.894
MMM* [41]	1.037	0.791	0.118	2.421
MoMask* [18]	0.898	0.440	0.106	2.516
GAITGen <sub>w/o-dis</sub>	0.569	0.222	0.076	2.475
GAITGen	<b>0.194</b>	<b>0.096</b>	<b>0.048</b>	<b>3.966</b>

Table 1. Comparison of GAITGen with baselines on the pathology-conditioned motion generation task. "\*" denotes baseline trained on PD-GaM. "

"" the closer to real the better.

from previous layers, conditioned on layer index n and severity  $c_p$ , to predict the current residuals, progressively enhancing fine-grained details. Each quantization layer has separate motion and pathology embeddings. Following Mo-Mask [18], parameter sharing is applied between successive layer embeddings within each token type, enhancing training efficiency while maintaining the distinct characteristics of motion and pathology tokens. The residual transformer minimizes the cross-entropy loss at each quantization layer:

$$\mathcal{L}_{\text{res}} = -\sum_{n=1}^{N} \sum_{\substack{i=1\\ \mathbf{h}: \neq \leq \text{MEND}>}}^{2T'+1} \log \mathcal{R}_{\theta}(\mathbf{h}_{k,i}^{(n)} \mid \mathbf{h}_{k}^{(0:n-1)}, c_{p}, n), \quad (10)$$

During training, quantization layer n is randomly selected for learning. In inference,  $\mathcal{R}_{\theta}$  begins with the embeddings from  $\mathcal{M}_{\theta}$ , sequentially predicts residual tokens, and updates the cumulative embedding over n steps. The final cumulative embedding is passed through the pretrained decoder to generate the final gait sequence. Since motion and pathology tokens are from separate codebooks, we define two distinct output heads for motion and pathology tokens prediction in both transformers.

Motion-Pathology Mix and Match Augmentation. Our disentangled representation space enables a novel Mix and Match data augmentation strategy, where motion features from one sample and pathology features from another can be combined to synthesize new gait sequences (Fig. 3). This allows us to apply the pathology profile of one individual to the motion dynamics of another. Given the scarcity of severe pathology cases in our dataset—a common challenge across datasets in this domain—we use this method to augment the severe class, enhancing diversity and improving training efficacy for our generative model.

#### 4. Experiments

Implementation Details. Model encoders are 1D convolutional ResNet blocks with a temporal downsampling rate of 4. The decoder  $\mathcal{D}$  mirrors the encoders' architecture.  $\mathcal{E}_m$  is pretrained for 200 epochs (learning rate (lr)  $2e^{-6}$ ) with a reduced lr factor of 0.1 during joint training with  $\mathcal{E}_p$  (lr  $2e^{-6})$  and the classifiers (lr  $2e^{-7})$  for 300 epochs. The loss weights are set as  $\lambda_r = 1$ ,  $\lambda_c = \lambda_{\rm adv} = 0.01$ , and  $\lambda_{\rm emb} = 0.02$ .

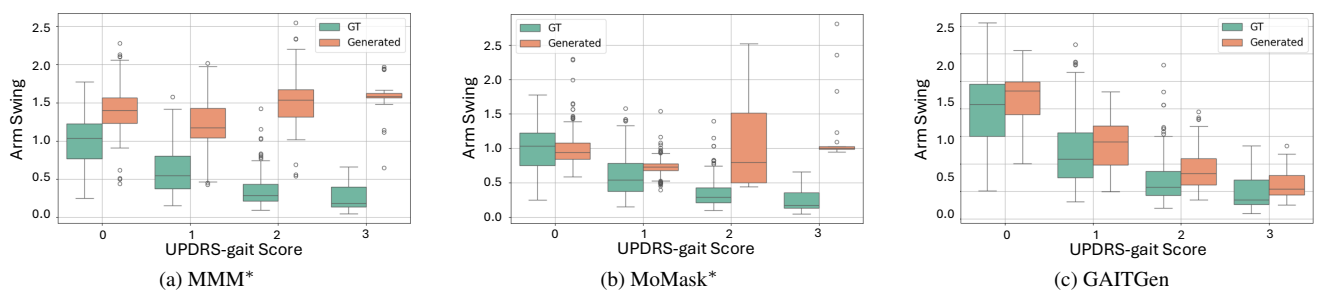


Figure 4. Comparison of arm-swing variability across MDS-UPDRS scores for GT and synthetic sequences.

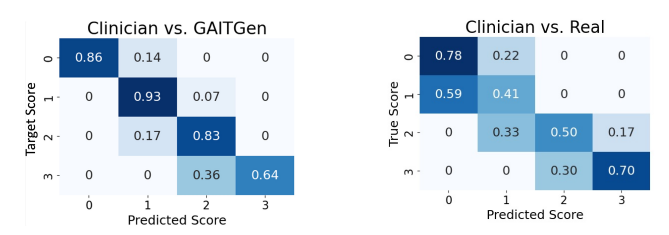


Figure 5. User study comparing clinician scoring of gait sequences with the true labels. True scores indicate (Left)-synthetic subset: condition given to GAITGen for sequence generation, (Right) Real subset: UPDRS-gait score provided by the PD-GaM dataset.

We adopt a quantization dropout strategy, with a probability of 0.2. N is set to 6, and both motion and pathology codebook dimensions are 64, with codebook sizes of 512 for motion and 128 for pathology with  $\alpha=1$  for the final model. For the  $\mathcal{M}_{\theta}$  and the  $\mathcal{R}_{\theta}$ , we use a lr of  $1e^{-3}$  with Adam schedule-free optimizers [11]. The mini-batch size is set to 512 for RVQ-VAE and 256 for the transformers.

#### 4.1. Datasets and Evaluation Metrics

**Dataset.** We introduce PD-GaM, a fully anonymized and publicly available dataset derived from PD4T [8]. Unlike the PD4T videos, which require ethics approval and request procedures, PD-GaM is readily available to the public. PD-GaM contains 1701 gait sequences from 30 individuals with PD, labeled with UPDRS-gait scores ranging from 0 to 3 by an expert (participants with a score of 4 are typically unable to walk without substantial assistance). Each video is segmented to include only gait segments, and SMPL parameters [30] are extracted using WHAM [48]. Post processing is applied to correct global trajectory artifacts introduced during mesh estimation. The dataset is split into training and validation sets based on participant IDs to ensure unbiased performance evaluation (details in supplement).

**Metrics.** Conventional metrics, such as FID, are unsuitable here due to limited data diversity and class imbalance, particularly for severe cases. FID requires a large, diverse sample set to reliably estimate distribution statistics [7], which PD dataset lacks. Instead, we use a set of clinically-relevant metrics to assess (*i*) generation quality, (*ii*) representation learning, and (*iii*) reconstruction fidelity.

(i)-Average Variance Error (AVE). Following [15, 40], we

use AVE, which measures the variance between generated and Ground Truth (GT) joints movements. It evaluates how closely the model replicates the expected variability in joint velocities over time, as observed in the GT for each class, assessing the fidelity of generated gait data. Absolute Armswing Mean Difference (AAMD) quantifies the variance between generated and GT arm-swing movements. A lower AAMD score indicates that generated sequences closely match the GT variance, accurately reflecting pathology-specific arm motion reduction typical in PD [23, 35]. Absolute Stooped Posture Mean Difference (ASMD) measures variance in torso inclination, capturing the stooped posture commonly observed in severe PD [23]. Following [17], Diversity (Div) assesses intra-class variability, measuring the diversity of gaits generated within each severity level.

(ii)—Pathology-Only Reconstruction Error (**PORE**) assesses the extent of motion information leakage into the pathology latent by comparing the Mean Per Joint Position Error (MPJPE) under two conditions: 1) reconstruction using only the pathology latent ( $\mathbf{q}_p$ ) and 2) reconstruction using both motion and pathology latents ( $\mathbf{q}_m + \mathbf{q}_p$ ). Let  $e_p$  and  $e_{pm}$  denote the MPJPEs for these conditions, with a preference for high  $e_p$  and low  $e_{pm}$ . The metric is calculated as

$$PORE = \frac{e_p - e_{pm}}{e_{pm} + \epsilon} \tag{11}$$

A higher PORE reflects more effective disentanglement with minimal motion information leakage into the pathology space. Pathology-Motion Predictive Gap (PMPG) assesses how well the latent spaces are separated by measuring the classification accuracy for pathology information in both pathology ( $\mathbf{q}_p$ ) and motion ( $\mathbf{q}_m$ ) latent codes. The score is calculated as the difference between the accuracy of the pathology classifier on  $\mathbf{q}_p$  and  $\mathbf{q}_m$ . A high PMPG indicates that pathology information is well captured in  $\mathbf{q}_p$  with minimal leakage into  $\mathbf{q}_m$ . Disentanglement Score (DS) provides a combined measure of the separation and is calculated as the geometric mean of PORE and PMPG. A higher DS indicates stronger disentanglement, with minimal leakage of motion information into the pathology latent and effective encoding of pathology characteristics.

(iii)—Similar to [6], we use **MPJPE** and **PAMPJPE** (Procrustes Aligned) to assess global and local reconstruction errors, and Acceleration Error (ACCL) for temporal quality.

Method	F1-score ↑	precision ↑	recall ↑
w/o synthetic data	0.67	0.72	0.69
+ MoMask* synthetic	0.51	0.59	0.49
+ our M&M synthetic	0.69	0.67	0.70
+ our GAITGen synthetic	0.73	0.79	0.71

Table 2. The effect of synthetic data on downstream UPDRS-gait classification. M&M denotes Mix and Match augmentation and \*indicates the model is trained on PD-GaM.

#### 4.2. Baseline Comparison

Since no existing baseline directly addresses the pathologyconditioned gait generation, we establish new baselines by adapting state-of-the-art motion generation models, Mo-Mask [18] and MMM [41], retraining them on our PD-GaM dataset for this task. 13k gait sequences are generated uniformly across 4 severity levels from each model. GAITGen consistently outperforms both baselines across all evaluation metrics (Tab. 1). Comparing GAITGen with a non-disentangled version of it (GAITGenwo-dis) underscores the necessity of disentanglement for capturing subtle, pathology-specific features. Here, GAITGen<sub>w/o-dis</sub> is trained only with one conditional encoder without the  $\mathcal{L}_{cls}$ and  $\mathcal{L}_{G-adv}$ . Fig. 4 illustrates the arm-swing distributions across severity levels for each method, showing that GAIT-Gen closely aligns with ground truth patterns and accurately reflects the reduction in arm-swing at higher severity levels, a result not achieved by the baseline models.

#### 4.3. Clinical User Study

To evaluate the clinical relevance of our synthetic gait sequences, we conducted a user study involving two specialist physicians and a research fellow experienced with PD. The clinicians were presented with 65 randomly selected video samples, comprising a mix of 34 real and 31 synthetic gait sequences. They were tasked with: (1) classifying each video as either real or synthetic, and (2) assigning a UPDRS-gait score (ranging from 0 to 3) to each video. The research fellow only conducted the first task. Results for each task were averaged across the two/three raters. The precision and recall for the first task were 0.52 and 0.57, respectively. This near chance performance suggests that GAITGen's outputs are visually realistic and challenging to distinguish from real gait patterns. Fig. 5-left compares clinician UPDRS-gait scores with that of the pathology condition provided to GAITGen during generation. The near diagonal confusion matrix highlights the effectiveness of GAITGen in matching the condition. Fig. 5–right compares clinician scores with UPDRS-gait scores provided in the PD-GaM dataset. Again, the matrix is nearly diagonal, and the differences are attributable to i) the somewhat subjective nature of the assessment, and ii) the fact that PD-GaM labels are based on the entire video sequences (including turns), while our clinician scores are only based on SMPL

Name	AuxClS	Comb.	$\mathcal{L}_{rec}$	$\mathbf{H}_{\mathbf{p}_{zero}}$	Pretrain	$\#cb_m,\!\#cb_p$
1CLS	$\phi_p$	conc	$\ell_1$	Х	Х	512,512
2CLS	$\phi_p, \psi_m$	conc	$\ell_1$	Х	X	512,512
AdaStyle	$\phi_p, \psi_m$	AdaLN	$\ell_1$	X	X	512,512
2CLS-cb <sub>p</sub> (128)	$\phi_p, \psi_m$	conc	$\ell_1$	Х	X	512, 128
GeoL1	$\phi_p, \psi_m$	conc	Geo+ $\ell_1$	Х	Х	512,128
ADD	$\phi_p, \psi_m$	add	Geo+ $\ell_1$	Х	Х	512,128
ADD- $\mathcal{H}_{zeroout}$	$\phi_p, \psi_m$	add	Geo+ $\ell_1$	1	X	512,128
GAITGen	$\dot{\phi_p}, \psi_m$	add	Geo+ $\ell_1$	✓	✓	512,128

Method		Reconstru	uction		Generation
Method	MPJPE ↓ 1	PAMPJPE .	↓ ACCL ↓	DS ↑	AVE ↓
1CLS	67.31	34.23	17.63	0.22	1.37
2CLS	92.29	59.06	30.51	0.34	1.45
AdaStyle	96.16	62.88	32.02	0.21	1.98
2CLS-cb <sub>p</sub> (128)	103.50	72.61	34.40	0.80	1.47
GeoL1	80.12	49.13	30.14	0.82	0.91
ADD	80.11	48.77	29.34	0.81	0.90
ADD- $\mathcal{H}_{zeroout}$	69.15	30.42	18.55	0.83	0.74
GAITGen	28.38	17.91	15.35	1.21	0.19
$\mathcal{E}_p$ - w/o $C_p$	31.04	18.32	19.95	0.81	0.34
w/o RQ	58.42	26.11	25.07	0.77	0.62

Table 3. Ablation for both reconstruction and generation tasks.

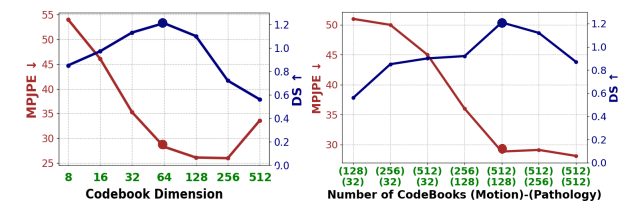


Figure 6. Evaluation of MPJPE and DS across various codebook dimensions and motion-pathology codebook sizes.

walking segments (excluding turns). The inter-rater agreement was measured using Weighted Kappa and Intraclass Correlation Coefficient (ICC). The Kappa value of 0.92 and ICC of 0.92 (95% CI [0.87, 0.95]) indicates almost perfect agreement between the two raters. Average raters' agreement with ground truth was 0.89. Notably, raters demonstrated higher agreement on the synthetic subset compared to the real subset (ICC 0.92 vs. 0.83). These results are in line with reliability ranges reported in prior research for UPDRS-gait [10, 44], underscoring the clinical applicability of GAITGen's synthetic data.

#### 4.4. Downstream task

To evaluate the utility of synthetic data generated by GAIT-Gen, we assess its impact on a downstream classification task for estimating parkinsonian severity. Tab. 2 compares model performance with various data sources: no synthetic data, MoMask\*-synthetic data, our Mix and Match augmented data, and GAITGen synthetic data, which was trained with Mix and Match augmentation included. For Mix and Match augmentation, we created 300 additional samples combining motion features from gait sequences with a UPDRS-gait score of 1 with pathology features from gaits with a score of 3 in the PD-GaM dataset, augmenting the underrepresented class 3, which slightly improved the classification results. For MoMask\* and GAITGen, we

(a) Synthetic Score 0 (b) Synthetic Score 1 (c) Synthetic Score 2 (d) Synthetic Score 3

Figure 7. Synthetic gait animations generated by GAITGen. (Best viewed with Acrobat Reader. Click the images to play the animations.)

(a) Real Score 1 (b) Real Score 3 (c) Mix and Match

Figure 8. (a) and (b) are two real samples from PD-GaM dataset with UPDRS-gait scores 1 and 3. Mix and Match sequence in (c) takes motion from (a) and pathology from (b). (Best viewed with Acrobat Reader. Click the images to play the animation clips.)

used each to generate 1000 synthetic sequences, 400 for class 3 and 200 for other classes to address class imbalance. Inclusion of GAITGen synthetic data achieves the highest F1-score, precision, and recall, while MoMask\* resulted in reduced performance.

#### 4.5. Ablation Studies

Ablation studies are conducted incrementally, adding one component at a time to evaluate the contributions of different components in the GAITGen (Tab. 3). Using a single classifier on the pathology latent (1CLS) results in moderate reconstruction performance but a low disentanglement score (DS) due to motion information leakage into the pathology latent. Introducing an adversarial classifier on the motion latent (2CLS) improves the DS, however, reconstruction errors increase, indicating a trade-off when relying solely on classification losses. Similarly, reducing the codebook size of the pathology (2CLS- $cb_p(128)$ ) enhances the DS by limiting its capacity to encode motion information. Expectedly, this adjustment increases reconstruction errors. To improve reconstruction, we zero out the pathology latent for healthy samples during training (ADD- $\mathcal{H}_{zeroout}$ ), forcing the motion encoder to capture all necessary motion information for healthy gait. This strategy enhances the DS slightly and reduces reconstruction errors considerably by ensuring that the motion encoder focuses on motion-related features without relying on the pathology latent. Combining this approach with pretraining the motion encoder yields the best performance across all metrics (GAITGen). We also perform an ablation treating pathology as a style using adaptive layer normalization (AdaStyle). It increases reconstruction errors and lowers DS. This confirms that modeling pathology as a style conflates motion and pathology features, making it challenging to control and synthesize gait sequences with specific pathology, especially for severe cases. Furthermore, using geodesic loss (GeoL1) significantly improves reconstruction metrics. This underscores the importance of respecting the non-Euclidean nature of rotations in SO(3), as Euclidean distances can lead to incorrect gradients.

Further ablations confirm using an unconditional pathology encoder  $(\mathcal{E}_p w/o C_p)$  decreases the DS and increases reconstruction errors. Conditioning pushes apart class representations in the pathology latent, enhancing separability between different severity levels. Finally, omitting Residual Vector Quantization (w/o RQ) degrades performance, confirming the importance of hierarchical quantization in capturing multi-level motion features. Fig. 6 presents the MPJPE and DS values across different codebook dimensions and motion-pathology codebook sizes. Best configurations are selected to balance high DS with low MPJPE, optimizing both disentanglement and reconstruction accuracy. Fig. 7 showcases synthetic sequences generated by GAITGen for each severity level. Fig. 8 presents a Mix and Match augmentation result, where motion features, such as curved walk in a gait with UPDRS score 1 (a) are combined with pathology features of a gait with score 3 (b), resulting in a more stooped posture, reduced arm swing, and shorter strides in (c). Unlike style transfer methods, this augmentation reflects severity-related constraints (e.g., shorter traversable distances typical of severe gait impairment for UPDRS-gait score 3). The balance between motion and pathology information is adjustable via the interference weight  $\alpha$ . Details are in the supplement.

#### 5. Conclusion

We proposed GAITGen, a novel model for generating clinically relevant gait sequences conditioned on pathology

severity by disentangling motion dynamics from pathologyspecific factors. Alongside GAITGen, we introduced PD-GaM, the largest 3D mesh Parkinsonian gait dataset, supporting clinical gait research. While our approach shows promise in capturing key features of parkinsonian gait and mitigating data scarcity, there remains significant potential for further exploration. Future work could integrate additional clinically relevant inputs, such as textual descriptions, by leveraging foundation models for supervision to enhance the richness of the generated data. Additionally, extending the model to include other manifestations of PD, such as tremors or dyskinesias, would provide a more comprehensive representation of the condition. Introducing controls over biomechanics and individual morphology, as explored in recent works like HUMOS [52], can further personalize gait synthesis and improve its applicability in clinical settings. These advancements can enhance GAITGen's potential integration into clinical practice, contributing to the development of tools for better diagnosis, monitoring, and treatment planning for movement disorders.

Acknowledgement. This work was supported in part by the Vector Institute for Artificial Intelligence; KITE – Toronto Rehabilitation Institute – University Health Network; the Data Sciences Institute at the University of Toronto; the Walter and Maria Schroeder Institute for Brain Innovation and Recovery; the Canadian Institutes of Health Research (CIHR); and the AMS Healthcare Fellowship in Compassion and Artificial Intelligence. The authors gratefully acknowledge the support of these institutions.

#### References

- [1] Kfir Aberman, Yijia Weng, Dani Lischinski, Daniel Cohen-Or, and Baoquan Chen. Unpaired motion style transfer from video to animation. *ACM Transactions on Graphics (TOG)*, 39(4):64–1, 2020. 2
- [2] Vida Adeli, Soroush Mehraban, Irene Ballester, Yasamin Zarghami, Andrea Sabo, Andrea Iaboni, and Babak Taati. Benchmarking skeleton-based motion encoder models for clinical applications: Estimating parkinson's disease severity in walking sequences. In 2024 IEEE 18th International Conference on Automatic Face and Gesture Recognition (FG), pages 1–10. IEEE, 2024. 1, 5
- [3] Sagie Benaim, Michael Khaitov, Tomer Galanti, and Lior Wolf. Domain intersection and domain difference. In *Proceedings of the IEEE/CVF International Conference on Computer Vision*, pages 3445–3453, 2019. 3
- [4] Ziyi Chang, Edmund JC Findlay, Haozheng Zhang, and Hubert PH Shum. Unifying human motion synthesis and style transfer with denoising diffusion probabilistic models. *arXiv* preprint arXiv:2212.08526, 2022. 2
- [5] Jorge Marquez Chavez and Wei Tang. A vision-based system for stage classification of parkinsonian gait using machine learning and synthetic data. Sensors, 22(12):4463, 2022. 3

- [6] Xin Chen, Biao Jiang, Wen Liu, Zilong Huang, Bin Fu, Tao Chen, and Gang Yu. Executing your commands via motion diffusion in latent space. In *Proceedings of the IEEE/CVF Conference on Computer Vision and Pattern Recognition*, pages 18000–18010, 2023. 2, 6, 4
- [7] Min Jin Chong and David Forsyth. Effectively unbiased fid and inception score and where to find them. In *Proceedings* of the IEEE/CVF conference on computer vision and pattern recognition, pages 6070–6079, 2020. 6
- [8] Amirhossein Dadashzadeh, Shuchao Duan, Alan Whone, and Majid Mirmehdi. PeCop: Parameter efficient continual pretraining for action quality assessment. In *Proceedings of* the IEEE/CVF Winter Conference on Applications of Computer Vision, pages 42–52, 2024. 1, 6
- [9] Wenxun Dai, Ling-Hao Chen, Jingbo Wang, Jinpeng Liu, Bo Dai, and Yansong Tang. MotionLCM: Real-time controllable motion generation via latent consistency model. arXiv preprint arXiv:2404.19759, 2024. 2
- [10] T de Deus Fonticoba, D Santos García, and M Macías Arribí. Inter-rater variability in motor function assessment in parkinson's disease between experts in movement disorders and nurses specialising in pd management. *Neurología (English Edition)*, 34(8):520–526, 2019. 2, 7
- [11] Aaron Defazio, Xingyu Alice Yang, Harsh Mehta, Konstantin Mishchenko, Ahmed Khaled, and Ashok Cutkosky. The road less scheduled. arXiv preprint arXiv:2405.15682, 2024. 6
- [12] Daniel Deng, Jill L Ostrem, Vy Nguyen, Daniel D Cummins, Julia Sun, Anupam Pathak, Simon Little, and Reza Abbasi-Asl. Interpretable video-based tracking and quantification of parkinsonism clinical motor states. *npj Parkinson's Disease*, 10(1):122, 2024. 1
- [13] Yao Feng, Jing Lin, Sai Kumar Dwivedi, Yu Sun, Priyanka Patel, and Michael J Black. ChatPose: Chatting about 3d human pose. In *Proceedings of the IEEE/CVF Conference* on Computer Vision and Pattern Recognition, pages 2093– 2103, 2024. 5
- [14] Yaroslav Ganin and Victor Lempitsky. Unsupervised domain adaptation by backpropagation. In *International conference* on machine learning, pages 1180–1189. PMLR, 2015. 5
- [15] Anindita Ghosh, Noshaba Cheema, Cennet Oguz, Christian Theobalt, and Philipp Slusallek. Synthesis of compositional animations from textual descriptions. In *Proceedings of* the IEEE/CVF international conference on computer vision, pages 1396–1406, 2021. 6
- [16] Christopher G Goetz, Barbara C Tilley, Stephanie R Shaftman, Glenn T Stebbins, Stanley Fahn, Pablo Martinez-Martin, Werner Poewe, Cristina Sampaio, Matthew B Stern, Richard Dodel, et al. Movement disorder society-sponsored revision of the unified parkinson's disease rating scale (MDS-UPDRS): scale presentation and clinimetric testing results. Movement disorders: official journal of the Movement Disorder Society, 23(15):2129–2170, 2008.
- [17] Chuan Guo, Shihao Zou, Xinxin Zuo, Sen Wang, Wei Ji, Xingyu Li, and Li Cheng. Generating diverse and natural 3d human motions from text. In *Proceedings of the IEEE/CVF Conference on Computer Vision and Pattern Recognition*, pages 5152–5161, 2022. 2, 6, 1

- [18] Chuan Guo, Yuxuan Mu, Muhammad Gohar Javed, Sen Wang, and Li Cheng. MoMask: Generative masked modeling of 3d human motions. In *Proceedings of the IEEE/CVF* Conference on Computer Vision and Pattern Recognition, pages 1900–1910, 2024. 2, 5, 7, 4
- [19] Irina Higgins, Loic Matthey, Arka Pal, Christopher P Burgess, Xavier Glorot, Matthew M Botvinick, Shakir Mohamed, and Alexander Lerchner. beta-VAE: Learning basic visual concepts with a constrained variational framework. *ICLR (Poster)*, 3, 2017. 3
- [20] Ting-Yao Hu, Mohammadreza Armandpour, Ashish Shrivastava, Jen-Hao Rick Chang, Hema Koppula, and Oncel Tuzel. SYNT++: Utilizing imperfect synthetic data to improve speech recognition. In ICASSP 2022-2022 IEEE International Conference on Acoustics, Speech and Signal Processing (ICASSP), pages 7682–7686. IEEE, 2022. 3
- [21] Siteng Huang, Biao Gong, Yutong Feng, Xi Chen, Yuqian Fu, Yu Liu, and Donglin Wang. Learning disentangled identifiers for action-customized text-to-image generation. In *Proceedings of the IEEE/CVF Conference on Computer Vision and Pattern Recognition*, pages 7797–7806, 2024. 3
- [22] Khawar Islam, Muhammad Zaigham Zaheer, Arif Mahmood, and Karthik Nandakumar. DiffuseMix: Label-preserving data augmentation with diffusion models. In Proceedings of the IEEE/CVF Conference on Computer Vision and Pattern Recognition, pages 27621–27630, 2024. 3
- [23] Joseph Jankovic. Parkinson's disease: clinical features and diagnosis. *Journal of neurology, neurosurgery & psychiatry*, 79(4):368–376, 2008. 2, 6
- [24] Jacob Devlin Ming-Wei Chang Kenton and Lee Kristina Toutanova. BERT: Pre-training of deep bidirectional transformers for language understanding. In *Proceedings of naacL-HLT*, page 2. Minneapolis, Minnesota, 2019. 5, 2
- [25] Kyungdo Kim, Sihan Lyu, Sneha Mantri, and Timothy W Dunn. TULIP: Multi-camera 3d precision assessment of parkinson's disease. In *Proceedings of the IEEE/CVF Con*ference on Computer Vision and Pattern Recognition, pages 22551–22562, 2024. 1
- [26] Renshuai Liu, Bowen Ma, Wei Zhang, Zhipeng Hu, Changjie Fan, Tangjie Lv, Yu Ding, and Xuan Cheng. Towards a simultaneous and granular identity-expression control in personalized face generation. In *Proceedings of the IEEE/CVF Conference on Computer Vision and Pattern Recognition*, pages 2114–2123, 2024. 3
- [27] Francesco Locatello, Gabriele Abbati, Thomas Rainforth, Stefan Bauer, Bernhard Schölkopf, and Olivier Bachem. On the fairness of disentangled representations. Advances in neural information processing systems, 32, 2019. 3
- [28] Francesco Locatello, Stefan Bauer, Mario Lucic, Gunnar Raetsch, Sylvain Gelly, Bernhard Schölkopf, and Olivier Bachem. Challenging common assumptions in the unsupervised learning of disentangled representations. In *interna*tional conference on machine learning, pages 4114–4124. PMLR, 2019. 3
- [29] Francesco Locatello, Michael Tschannen, Stefan Bauer, Gunnar Rätsch, Bernhard Schölkopf, and Olivier Bachem. Disentangling factors of variation using few labels. arXiv preprint arXiv:1905.01258, 2019. 3

- [30] Matthew Loper, Naureen Mahmood, Javier Romero, Gerard Pons-Moll, and Michael J. Black. SMPL: A skinned multi-person linear model. *ACM Trans. Graphics (Proc. SIGGRAPH Asia)*, 34(6):248:1–248:16, 2015. 6
- [31] Mandy Lu, Kathleen Poston, Adolf Pfefferbaum, Edith V Sullivan, Li Fei-Fei, Kilian M Pohl, Juan Carlos Niebles, and Ehsan Adeli. Vision-based estimation of MDS-UPDRS gait scores for assessing parkinson's disease motor severity. In Medical Image Computing and Computer Assisted Intervention–MICCAI 2020: 23rd International Conference, Lima, Peru, October 4–8, 2020, Proceedings, Part III 23, pages 637–647. Springer, 2020. 1
- [32] Mandy Lu, Qingyu Zhao, Kathleen L Poston, Edith V Sullivan, Adolf Pfefferbaum, Marian Shahid, Maya Katz, Leila Montaser Kouhsari, Kevin Schulman, Arnold Milstein, et al. Quantifying parkinson's disease motor severity under uncertainty using MDS-UPDRS videos. *Medical image* analysis, 73:102179, 2021. 1
- [33] Naureen Mahmood, Nima Ghorbani, Nikolaus F Troje, Gerard Pons-Moll, and Michael J Black. Amass: Archive of motion capture as surface shapes. In *Proceedings of the IEEE/CVF international conference on computer vision*, pages 5442–5451, 2019. 1
- [34] Sina Mehdizadeh, Hoda Nabavi, Andrea Sabo, Twinkle Arora, Andrea Iaboni, and Babak Taati. The toronto older adults gait archive: video and 3d inertial motion capture data of older adults' walking. *Scientific data*, 9(1):398, 2022. 1
- [35] Anat Mirelman, Hagar Bernad-Elazari, Avner Thaler, Eytan Giladi-Yacobi, Tanya Gurevich, Mali Gana-Weisz, Rachel Saunders-Pullman, Deborah Raymond, Nancy Doan, Susan B Bressman, et al. Arm swing as a potential new prodromal marker of parkinson's disease. *Movement Disorders*, 31(10):1527–1534, 2016. 6
- [36] Meg E Morris, Robert Iansek, Thomas A Matyas, and Jeffery J Summers. The pathogenesis of gait hypokinesia in parkinson's disease. *Brain*, 117(5):1169–1181, 1994. 2
- [37] Koichiro Niinuma, Itir Onal Ertugrul, Jeffrey F Cohn, and László A Jeni. Synthetic expressions are better than real for learning to detect facial actions. In *Proceedings of the IEEE/CVF Winter Conference on Applications of Computer Vision*, pages 1248–1257, 2021. 3
- [38] Hyun-Jic Oh and Won-Ki Jeong. DiffMix: Diffusion model-based data synthesis for nuclei segmentation and classification in imbalanced pathology image datasets. In *International Conference on Medical Image Computing and Computer-Assisted Intervention*, pages 337–345. Springer, 2023. 3
- [39] Mathis Petrovich, Michael J Black, and Gül Varol. Actionconditioned 3d human motion synthesis with transformer vae. In *Proceedings of the IEEE/CVF International Con*ference on Computer Vision, pages 10985–10995, 2021. 2
- [40] Mathis Petrovich, Michael J. Black, and Gül Varol. TEMOS: Generating diverse human motions from textual descriptions. In European Conference on Computer Vision (ECCV), 2022.
- [41] Ekkasit Pinyoanuntapong, Pu Wang, Minwoo Lee, and Chen Chen. MMM: Generative masked motion model. In Pro-

- ceedings of the IEEE/CVF Conference on Computer Vision and Pattern Recognition, pages 1546–1555, 2024. 2, 5, 7
- [42] Matthias Plappert, Christian Mandery, and Tamim Asfour. The kit motion-language dataset. *Big data*, 4(4):236–252, 2016.
- [43] Rahm Ranjan, David Ahmedt-Aristizabal, Mohammad Ali Armin, and Juno Kim. Computer vision for clinical gait analysis: A gait abnormality video dataset. *arXiv preprint arXiv:2407.04190*, 2024. 1, 2
- [44] Marcus Richards, Karen Marder, Lucien Cote, and Richard Mayeux. Interrater reliability of the unified parkinson's disease rating scale motor examination. *Movement Disorders*, 9(1):89–91, 1994. 2, 7
- [45] Karl Ridgeway and Michael C Mozer. Learning deep disentangled embeddings with the f-statistic loss. *Advances in neural information processing systems*, 31, 2018. 3
- [46] Andrea Sabo, Andrea Iaboni, Babak Taati, Alfonso Fasano, and Carolina Gorodetsky. Evaluating the ability of a predictive vision-based machine learning model to measure changes in gait in response to medication and dbs within individuals with parkinson's disease. *BioMedical Engineering* OnLine, 22(1):120, 2023. 1
- [47] Mert Bülent Sarıyıldız, Karteek Alahari, Diane Larlus, and Yannis Kalantidis. Fake it till you make it: Learning transferable representations from synthetic imagenet clones. In *Proceedings of the IEEE/CVF Conference on Computer Vision and Pattern Recognition*, pages 8011–8021, 2023. 3
- [48] Soyong Shin, Juyong Kim, Eni Halilaj, and Michael J. Black. WHAM: Reconstructing world-grounded humans with accurate 3D motion. In *IEEE/CVF Conf. on Computer Vision and Pattern Recognition (CVPR)*, 2024. 6, 1
- [49] Wenfeng Song, Xingliang Jin, Shuai Li, Chenglizhao Chen, Aimin Hao, Xia Hou, Ning Li, and Hong Qin. Arbitrary motion style transfer with multi-condition motion latent diffusion model. In *Proceedings of the IEEE/CVF Conference on Computer Vision and Pattern Recognition*, pages 821–830, 2024. 2
- [50] Tianxin Tao, Xiaohang Zhan, Zhongquan Chen, and Michiel van de Panne. Style-ERD: Responsive and coherent online motion style transfer. In *Proceedings of the IEEE/CVF Con*ference on Computer Vision and Pattern Recognition, pages 6593–6603, 2022. 2
- [51] Guy Tevet, Sigal Raab, Brian Gordon, Yoni Shafir, Daniel Cohen-or, and Amit Haim Bermano. Human motion diffusion model. In *The Eleventh International Conference on Learning Representations*, 2023. 2, 4
- [52] Shashank Tripathi, Omid Taheri, Christoph Lassner, Michael Black, Daniel Holden, and Carsten Stoll. HUMOS: Human motion model conditioned on body shape. In *European Conference on Computer Vision*, pages 133–152. Springer, 2025.
- [53] Sjoerd Van Steenkiste, Francesco Locatello, Jürgen Schmidhuber, and Olivier Bachem. Are disentangled representations helpful for abstract visual reasoning? *Advances in neural in*formation processing systems, 32, 2019. 3
- [54] Tan Wang, Linjie Li, Kevin Lin, Yuanhao Zhai, Chung-Ching Lin, Zhengyuan Yang, Hanwang Zhang, Zicheng Liu,

- and Lijuan Wang. DisCo: Disentangled control for realistic human dance generation. In *Proceedings of the IEEE/CVF Conference on Computer Vision and Pattern Recognition*, pages 9326–9336, 2024. 3
- [55] Yaohui Wang, Piotr Bilinski, Francois Bremond, and Antitza Dantcheva. G3AN: Disentangling appearance and motion for video generation. In *Proceedings of the IEEE/CVF Con*ference on Computer Vision and Pattern Recognition, pages 5264–5273, 2020. 3
- [56] Zhizhong Wang, Lei Zhao, and Wei Xing. StyleDiffusion: Controllable disentangled style transfer via diffusion models. In *Proceedings of the IEEE/CVF International Conference on Computer Vision*, pages 7677–7689, 2023. 3
- [57] Zhicai Wang, Longhui Wei, Tan Wang, Heyu Chen, Yanbin Hao, Xiang Wang, Xiangnan He, and Qi Tian. Enhance image classification via inter-class image mixup with diffusion model. In *Proceedings of the IEEE/CVF Conference* on Computer Vision and Pattern Recognition, pages 17223– 17233, 2024. 3
- [58] Will Williams, Sam Ringer, Tom Ash, David MacLeod, Jamie Dougherty, and John Hughes. Hierarchical quantized autoencoders. Advances in Neural Information Processing Systems, 33:4524–4535, 2020. 3
- [59] Qiucheng Wu, Yujian Liu, Handong Zhao, Ajinkya Kale, Trung Bui, Tong Yu, Zhe Lin, Yang Zhang, and Shiyu Chang. Uncovering the disentanglement capability in textto-image diffusion models. In Proceedings of the IEEE/CVF conference on computer vision and pattern recognition, pages 1900–1910, 2023. 3
- [60] Yiming Xie, Varun Jampani, Lei Zhong, Deqing Sun, and Huaizu Jiang. OmniControl: Control any joint at any time for human motion generation. arXiv preprint arXiv:2310.08580, 2023.
- [61] Zikang Xu, Jun Li, Qingsong Yao, Han Li, Mingyue Zhao, and S Kevin Zhou. Addressing fairness issues in deep learning-based medical image analysis: a systematic review. npj Digital Medicine, 7(1):286, 2024. 1
- [62] Wenjie Yin, Hang Yin, Kim Baraka, Danica Kragic, and Mårten Björkman. Dance style transfer with cross-modal transformer. In Proceedings of the IEEE/CVF Winter Conference on Applications of Computer Vision, pages 5058–5067, 2023. 2
- [63] Jianrong Zhang, Yangsong Zhang, Xiaodong Cun, Yong Zhang, Hongwei Zhao, Hongtao Lu, Xi Shen, and Ying Shan. Generating human motion from textual descriptions with discrete representations. In *Proceedings of the IEEE/CVF conference on computer vision and pattern recognition*, pages 14730–14740, 2023. 2, 5
- [64] Mingyuan Zhang, Huirong Li, Zhongang Cai, Jiawei Ren, Lei Yang, and Ziwei Liu. FineMoGen: Fine-grained spatiotemporal motion generation and editing. Advances in Neural Information Processing Systems, 36:13981–13992, 2023. 2
- [65] Yi Zhou, Connelly Barnes, Jingwan Lu, Jimei Yang, and Hao Li. On the continuity of rotation representations in neural networks. In *Proceedings of the IEEE/CVF conference on* computer vision and pattern recognition, pages 5745–5753, 2019. 4

[66] Zixiang Zhou, Yu Wan, and Baoyuan Wang. AvatarGPT: All-in-one framework for motion understanding planning generation and beyond. In *Proceedings of the IEEE/CVF Conference on Computer Vision and Pattern Recognition*, pages 1357–1366, 2024. 5

### **Appendix**

**Supplemental Video.** Our model generates gait sequences that depict the movement impairments associated with PD. The supplemental video provides qualitative demonstrations that illustrate these motion dynamics and subtle PD-related features in a way that still images cannot. We strongly recommend that readers view the provided supplemental video.

Further clarification on "Motion" and "Pathology" terms. In our work, "Motion" denotes the *general* gait biomechanics (e.g., alternating heel strikes) or the inherent physiological motion constraints (e.g., limited range of motion in knee flexion and extension). "Pathology", on the other hand, describes disease-specific patterns absent in healthy gait (e.g., small, shuffling steps, reduced arm swing, festination, etc.). Our model explicitly separates these factors by learning a distinct pathology latent space, ensuring that pathology-related deviations are captured independently of normal motion dynamics. This disentanglement allows for precise control over gait synthesis, enabling pathology-conditioned generation while preserving natural locomotion patterns.

#### A. Elaboration on Clinical Motivation

Parkinsonian gait analysis has direct clinical relevance, particularly in early detection and continuous monitoring. Yet, the scarcity of annotated data for severe PD stages—where motor symptoms become most pronounced—restricts the ability of machine learning models to generalize [2]. Our synthetic generation approach mitigates this data imbalance by creating realistic, pathology-specific gait samples. This enriched training set ultimately supports more robust detection and staging tools, which could improve clinical workflows and inform therapeutic decisions without requiring extensive additional data collection. This approach could also reduce the burden of collecting large amounts of new clinical data.

#### **B. PD-GaM Dataset**

PD-GaM is a large PD Gait 3D Mesh dataset derived from the PD4T dataset; but it is anonymized for public release. The original PD4T dataset included 426 gait video recordings from 30 individuals with PD. Each participant in PD4T was asked to walk forward and backward twice, resulting in 4 walking segments per participant. Each recording was reviewed and segmented to retain usable gait segments while excluding frames involving turns. Turns present a unique challenge for individuals with PD, as the gait changes ob-

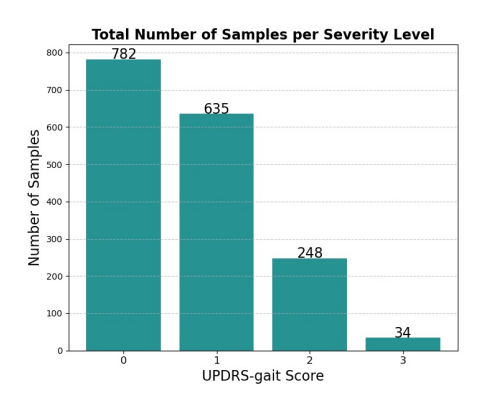


Figure S7. Histogram of UPDRS-gait scores in our PD-GaM dataset.

served during turns differ significantly from those seen during walking. To maintain a consistent representation of gait patterns, only walking sequences are included in this paper. However, we plan to also release the turn segments in PD-GaM to support research on turn-specific gait analysis. SMPL parameters for each subject were extracted at 25 FPS using the WHAM [48]. The camera, positioned at eye level and following the subjects as they walked in original videos, introduced minor distortions in global trajectories. These distortions were corrected during preprocessing to minimize global position artifacts. The dataset is divided into training (1253 samples) and test (448 samples) sets using a participant-based split to ensure unbiased evaluation. A histogram of UPDRS-gait scores in PD-GaM is presented in Fig. S7, highlighting the imbalance in class representation, particularly the limited number of samples in the severe category (class 3). This scarcity emphasizes the importance of our Mix and Match augmentation strategy.

#### C. Input Motion Representation

Our motion representation follows the HumanML3D format [17]. Each frame is encoded as a 263-dimensional vector derived from the SMPL mesh representation of WHAM [48], with joints mapped to 22 AMASS joints [33]. This representation includes root angular velocity  $(r^a \in \mathbb{R})$  along the Y-axis, root linear velocities  $(r^x, r^z \in \mathbb{R})$  on the XZ-plane, root height  $(r^y \in \mathbb{R})$ , local joint positions  $(j^p \in \mathbb{R}^{3N_j})$ , joint velocities  $(j^v \in \mathbb{R}^{3N_j})$ , joint rotations  $(j^r \in \mathbb{R}^{6N_j})$ , and binary foot-ground contact features  $(c^f \in \mathbb{R}^4)$ . This redundant representation captures both kinematic and dynamic properties, making it suitable for

neural models, particularly generative frameworks. It also allows for the disentanglement of motion dynamics from pathology-specific characteristics.

#### D. Mix and Match Augmentation.

Mix and Match augmentation is not a naive data augmentation technique. It leverages the decoder's capacity to integrate motion and pathology features. The decoder determines the final output by considering the input motion, the pathology severity level, and their likelihoods, resulting in coherent and realistic gait sequences. For instance, in qualitative results shown in Fig.8 (manuscript), when a severe pathology (score 3) is paired with a motion where the person walks a long distance, the decoder adapts the trajectory to reflect the constraints of severe pathology, which typically limits walking distance. This demonstrates that our method goes beyond naive augmentation by producing contextually appropriate modifications based on the severity level. However, while Mix and Match is effective for augmenting underrepresented classes, it is limited in diversity and control. It serves as a supplementary technique suitable for small-scale augmentation but does not replace the need for training our generative model.

# E. Additional Implementation Details and Experiments.

We employ a 1D convolutional ResNet-based encoder-decoder for gait sequence modeling. The encoder down-samples the input sequence through two convolutional ResNet blocks, reducing the temporal resolution by  $4\times$ . Initially, a conv layer maps the D-dimensional input motion to  $D_m=D_p=64$  channels, followed by temporal downsampling and quantization into  $\# \operatorname{cb}_m=512$  motion and  $\# \operatorname{cb}_p=128$  pathology codebooks, each with 64-dimensional embeddings. The decoder mirrors the encoder to reconstruct the motion sequence using upsampling ResNet blocks, thereby restoring the original temporal resolution. It also includes one conv layer to recover the original channel size.

To ensure diversity in generated sequences, GAITGen integrates residual stochastic sampling techniques, inspired by language modeling approaches such as BERT [24]. During inference, we apply Top-K filtering and remasking plus Gumbel sampling to enhance diversity. Specifically, in an iterative 10-step process, the top 10% of predicted tokens are retained (based on predicted probabilities), while the remaining 90% are re-masked for refinement. During training, we introduce additional stochasticity by replacing selected masked tokens with random tokens 8% of the time instead of <code><mask></code> to enhance robustness. We used CLIP encoding followed by a projection layer for condition, with the four-class  $c_p$  functioning similarly to action or style con-

ditioned motion generation [39, 49].

Number of Quantization Layer. Tab. S7 shows that increasing the number of quantization layers from 1 to 6 leads to consistent improvements in reconstruction metrics and generation quality (lower AVE). This is because additional layers allow the model to capture finer-grained details of the gait sequences. However, beyond 6 layers, we observe marginal gains in reconstruction and a slight decline in generation performance. This may be due to the increased complexity, making it more challenging for the residual transformer  $\mathcal{R}_{\theta}$  to predict higher-order residuals effectively. Additionally, more layers introduce higher computational costs with diminished disentanglement (lower DS) without significant benefits. Therefore, we selected 6 quantization layers for GAITGen as it offers a good trade-off between reconstruction fidelity and generation quality.

#Quantization		Reconstruc	tion		Generation
layer(s)	MPJPE ↓	PAMPJPE ↓	ACCL ↓	DS↑	AVE ↓
1	58.42	26.11	25.07	0.77	0.62
2	51.78	24.56	22.43	0.92	0.46
3	43.90	21.87	19.76	1.15	0.47
4	35.77	19.98	17.43	1.02	0.32
5	31.83	18.51	15.67	1.24	0.24
6	28.38	17.91	15.35	1.21	0.19
7	27.92	17.12	15.11	0.95	0.21
8	27.15	16.94	15.14	0.88	0.25

Table S7. Impact of the number of quantization layers on model performance.

Motion Encoder Reduced Learning Rate Factor. We examine how reducing the learning rate (lr) of the motion encoder  $\mathcal{E}_m$  during fine-tuning with the pathology encoder influences disentanglement. As shown in Tab. S8, using an lr reduction factor of 0.1 increases the DS from 0.94 to 1.21. With an lr factor of 1 (no reduction), the motion encoder updates quickly under the influence of the adversarial classifier, causing it to unlearn essential motion features, which degrades reconstruction quality. To compensate, the pathology encoder begins capturing motion information, compromising disentanglement and reducing the DS. Conversely, very small lr factors (0.01 and 0.001) lead to insufficient adjustments by the motion encoder, leaving residual pathology information in the motion latent space and resulting in a lower DS.

$\mathcal{E}_m$ lr factor	MPJPE ↓	PAMPJPE ↓	ACCL ↓	DS ↑
1	28.19	17.84	15.31	0.94
0.1	28.38	<u>17.91</u>	<u>15.35</u>	1.21
0.01	28.71	18.23	17.01	1.11
0.001	29.94	19.29	17.06	0.86

Table S8. Impact of learning rate reduction factors for the motion encoder  $\mathcal{E}_m$  during fine-tuning. Best results are in **bold**, comparable results are underlined.

#### Number of Inference Iterations and Masking Scheduler.

Here we investigate how the number of inference iterations and the choice of scheduler influence the performance of the Mask Transformer  $\mathcal{M}_{\theta}$ . During iterative refinement, the masking ratio  $\beta(t)$  determines the proportion of tokens to re-mask at each iteration, with t representing the normalized timestep from 0 to 1 over R iterations (i.e.,  $t=rac{ ext{current iteration}}{R}$ ). Two schedulers are compared: the linear scheduler  $(\beta(t) = 1 - t)$  decreases the masking ratio uniformly, while the cosine scheduler  $(\beta(t) = \cos(\frac{\pi t}{2}))$  maintains a higher masking ratio initially, gradually reducing it in later iterations. This higher masking ratio allows the cosine scheduler to focus on easier-to-predict tokens first and progressively tackle harder tokens in later iterations. During training, t is sampled uniformly  $(t \sim \mathcal{U}(0,1))$ , and during inference, t is deterministically stepped from 0 to 1 over R iterations. At each iteration, the number of tokens to be masked is calculated as  $\beta(t) \times M$ , where M = 2T' + 1 is the total number of tokens in the sequence. Tab. \$9 shows that the cosine scheduler consistently outperforms the linear one, especially at fewer iterations, indicating faster convergence.

#Iterations (Scheduler)	AVE ↓	<b>AAMD</b> ↓	ASMD ↓	$\mathbf{Div} \rightarrow$
5 (linear)	0.367	0.165	0.071	3.744
10 (linear)	0.294	0.142	0.049	3.906
20 (linear)	0.217	0.103	0.051	3.911
5 (cosine)	0.313	0.134	0.066	3.824
10 (cosine)	0.194	0.096	0.048	3.966
20 (cosine)	0.194	0.099	0.047	3.957

Table S9. Impact of inference iterations and scheduler type of the mask transformer model.

VAE Channel Size. The channel size in the VAE determines the number of feature channels in intermediate layers, influencing model's representational capacity. Experiments with varying channel sizes (Tab. S10) show a channel size of 512 achieves the best overall performance, outperforming smaller channel sizes. Increasing the size to 1024 marginally improves ACCL but comes at the cost of increased computational complexity without meaningful benefits to other metrics.

$\mathcal{E}_m$ #Channel	MPJPE ↓	PAMPJPE ↓	ACCL↓	DS↑
128	58.31	27.65	25.98	0.76
256	39.08	21.78	19.97	0.94
512	28.38	17.91	15.35	1.21
1024	29.12	17.95	15.23	1.14

Table S10. Impact of VAE channel size on model performance.

**Interference Weight.** The interference weight  $\alpha$  modulates the contribution of pathology-specific features in the reconstructed gait sequences. Experiments with  $\alpha = 0.2, 0.5, 1.0$ 

revealed a trade-off: Lower values of  $\alpha$  prioritize motion dynamics over pathology features, slightly improving reconstruction, but reducing classification accuracy of  $\phi_p$  for severe pathology (UPDRS-gait score 3). Fig. S8 presents the confusion matrices of the classifier  $\phi_p$  for different  $\alpha$  values. Our final model uses  $\alpha=1.0$  to to achieve better performance on severe cases, while  $\alpha$  remains adjustable depending on specific application requirements.

Findings on Codebook Learning. We conducted an experiment to examine the effects of increasing the codebook commitment loss weight  $(\lambda_{emb})$  and incorporating periodic codebook reset strategy [58] in the quantization process. Raising  $\lambda_{emb}$  from 0.02 to 0.09 resulted in stronger commitment of input vectors to specific codebook entries. However, this came at the cost of worse reconstruction quality and severity prediction performance from pathology latents  $\mathbf{q}_p$ . A higher  $\lambda_{emb}$  caused the model to commit to a subset of codebook entries early, leaving others unused. We also experimented with periodic codebook resets, where unused codebook entries are reset to random values every 20 iterations instead of at every iteration, giving the codebooks more opportunity to be used before being reset. However, we found that the introduction of new, randomly initialized entries after multiple iterations disrupted the model's established encoding patterns, leading to instability and degraded performance. In contrast, when using a lower  $\lambda_{emb}$  (0.02) with codebook resets at every iteration, the model's commitment to codebook entries was less rigid, allowing the model to adapt more smoothly to the resets without significant disruption, resulting in the most optimal performance.

#### F. Latent space visualization

We present UMAP visualizations of the latent space in Fig. S9. GAITGen achieves well-clustered latent representations aligned with UPDRS-gait scores. Without condition ( $\mathcal{E}_p$ ) or disentanglement, the clusters displays significant overlap among classes.

#### G. Metric Details

Here we provide details of the AVE, AAMD, and ASMD metrics. All reported generation results are averaged over 10 repetitions.

**Average Variance Error (AVE)** measures how closely the variance of local joint positions in the generated poses matches the ground-truth variance. For each joint j, the variance  $\sigma[j]$  is computed as:

$$\sigma[j] = \frac{1}{T - 1} \sum_{t \in T} \left( P_t[j] - \bar{P}[j] \right)^2 \tag{5}$$

where  $\bar{P}[j]$  is the mean position for joint j across T frames.

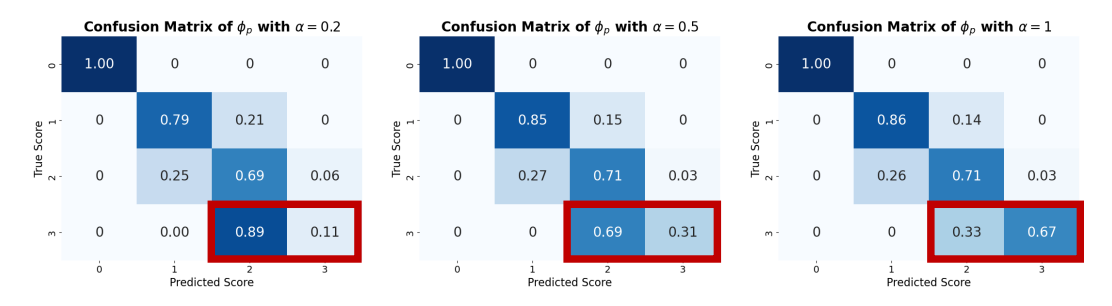


Figure S8. Confusion matrices of the classifier  $\phi_p$  for different values of interference weight  $\alpha$ .

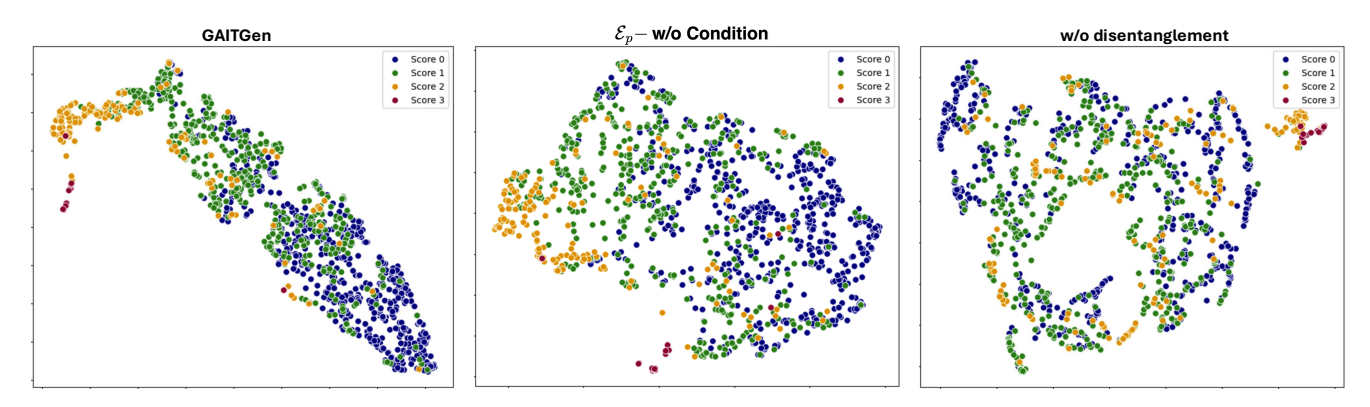


Figure S9. UMAP visualizations of the latent space representations under different settings. The left panel shows GAITGen with well-clustered latent representations aligned with UPDRS-gait scores. The middle panel represents the latent space when  $\mathcal{E}_p$  is unconditional, exhibiting overlap among classes. The right panel shows the results without disentanglement, further highlighting increased overlap and less separation of latent clusters.

The AVE for each joint is then defined as:

$$AVE[j] = \frac{1}{N} \sum_{\sigma \in N} \|\sigma[j] - \hat{\sigma}[j]\|_2$$
 (6)

where  $\sigma[j]$  and  $\hat{\sigma}[j]$  are the variances of joint j in the ground-truth and generated poses, respectively. The overall AVE is obtained by averaging the per-joint AVE values. Absolute Arm Swing Mean Difference (AAMD) measures how closely the generated gait sequences replicate the arm swing ranges of the ground-truth data across different severity classes. For each class c, we calculate the mean arm swing range for the ground-truth  $(\overline{AS}_{gt}^{(c)})$  and the generated  $(\overline{AS}_{gen}^{(c)})$  sequences. The arm swing range for each sequence is computed by measuring the Euclidean distances between the wrist and shoulder joints at each time step, finding the maximum and minimum distances over the sequence, normalizing by leg length, and selecting the minimum arm swing between the two arms. The AAMD is then defined as the average of the absolute differences between these class-wise mean arm swing ranges:

$$AAMD = \frac{1}{C} \sum_{c=1}^{C} \left| \overline{AS}_{gen}^{(c)} - \overline{AS}_{gt}^{(c)} \right|$$
 (7)

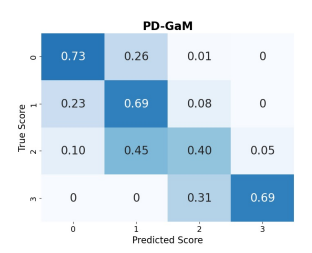
where C is the total number of classes. A lower AAMD indicates that the generated sequences closely match the real arm swing patterns.

Absolute Stooped Posture Mean Difference (ASMD) quantifies how well the generated gait sequences replicate the stooped posture characteristic across different classes. Similar to AAMD, for each class, we compute the mean stooped posture for the ground-truth  $(\overline{SP}_{gt}^{(c)})$  and generated  $(\overline{SP}_{gen}^{(c)})$  sequences by calculating the vertical distance between the neck and sacrum joints at each time step for each sequence, averaging these distances over all frames, and normalizing by leg length. The ASMD is defined as the average of the absolute differences between these class-wise mean stooped postures:

$$ASMD = \frac{1}{C} \sum_{c=1}^{C} \left| \overline{SP}_{gen}^{(c)} - \overline{SP}_{gt}^{(c)} \right|$$
 (8)

# H. User Study and Downstream Task Confusion Matrices

For the downstream classification task, we used a convolutional movement encoder, pre-trained on motion data from established motion generation benchmarks [6, 18, 51],



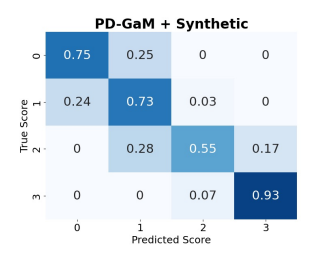


Figure S10. Confusion matrix of downstream classifiers trained on (left) PD-GaM (right) PD-GaM+Synthetic data.

Real	0.52	0.48
synthetic (GAITGen)	0.48	0.52
	Judged as real	Judged as synthetic

Figure S11. User study on distinguising real vs. synthetic data generated by GAITGen.

known for reliably capturing fine-grained motion features. Motion embeddings extracted from this encoder are fed into a lightweight trainable classifier head with three fully connected layers to predict UPDRS-gait severity levels. The classifier is trained on the PD-GaM training set along with synthetic data and evaluated *only* on real samples from the PD-GaM test split. The confusion matrices in Fig. S10 compare the classifier performance when trained on (left) the PD-GaM training set alone (right) PD-GaM combined with synthetic data, both tested on the same real PD-GaM test set. To rule out potential classifier-specific effects, we also tested the best classifier from [2] and F1-score improved from 62% to 69% (+7%) with synthetic data, further confirming augmentation benefits across classifiers.

Fig. S11 shows the confusion matrix for the real vs. synthetic classification task in the clinical user study described in the main manuscript. The near chance-level performance by clinicians highlights the high visual realism of GAIT-Gen's outputs.

#### I. Limitations

The current dataset scoring is based on gait segments that also include turning task, which may influence the UPDRS-gait scores. To address this, we are preparing revised scores focused exclusively on walking segments and will release both formats to accommodate different research objectives. Additionally, the dataset exhibits class imbalance, particularly in severe pathology cases with limited samples. Although our augmentation strategy helped mitigate this issue, integrating additional datasets standardized to the PD-GaM format could enhance generalizability and diversity of the generated sequences. Finally, while our model is tailored to PD gait patterns, its applicability to other abnormalities remains an area for future exploration.